RSC Advances

PAPER

View Article Online
View Journal | View Issue

Cite this: *RSC Adv.*, 2015, **5**, 12358

The effect of thermal annealing on the optical and electrical properties of ZnO epitaxial films grown on n-GaAs (001)

Wei-Rein Liu,*[a] Bi-Hsuan Lin,[a] Chi-Yuan Lin,[b] Song Yang,[a] Chin-Chia Kuo,[b] Forest Shih-Sen Chien,[c] Chen-Shiung Chang,[b] Chia-Hung Hsu*[ab] and Wen-Feng Hsieh[b]

Received 4th November 2014
Accepted 15th January 2015

DOI: 10.1039/c4ra13771j

www.rsc.org/advances

Wurtzite ZnO epitaxial layers grown on n-type GaAs (001) by pulsed laser deposition (PLD) exhibited n-type conductivity. Post-growth annealing leads the conversion of carrier type from electron to hole, as revealed by Hall effect measurements, although only moderate structural improvement was observed. The carrier type conversion is attributed to thermally activated arsenic diffusion from the substrate, confirmed by secondary ion mass spectrometry and photoluminescence. The surface electrical properties of both the as-deposited n-type and annealed p-type ZnO epitaxial layers were thoroughly characterized by Kelvin force microscopy (KFM) and electrostatic force microscopy (EFM). The results indicated the existence of a high density of surface states close to the ZnO midgap with a density of a few 10^{14} cm^{-2} eV^{-1}. The Fermi levels (E_F) of n- and p-type ZnO epitaxial layers were found to be 1.06 eV below the conduction-band minimum (CBM) and 1.612–1.769 eV above the valence-band maximum (VBM), respectively. The small E_F difference between the n- and p-type ZnO epitaxial layers implies Fermi level pinning at the surface of both n- and p-type ZnO epitaxial layers.

Introduction

ZnO, a II–VI compound semiconductor, is a promising material for high efficiency light-emitting devices and for optical applications in UV luminescence due to its wide direct band gap, 3.37 eV, and large exciton binding energy, 60 meV at 295 K. However, because of the asymmetric doping limitations and the compensation effect caused by native defects, such as O_i and V_{Zn} which play a role as hole killer, reliable p-type ZnO is difficult to attain.[1,2] How to fabricate high quality and stable p-type ZnO epitaxial films thus remains the major obstacle to the realization of ZnO-based photoelectronic devices.

To achieve p-type ZnO, various doping approaches, such as group V elements (N,[3] P,[4] As,[5] and Sb[6]) substituting for O, group I elements (Li[7] and Ag[8]) for Zn, donor–acceptor co-doping, with group III and group V elements simultaneous substituting for Zn and O,[9] and dual-acceptor co-doping, with group I and group V elements substituting for Zn and O simultaneously,[10] have been explored in recent years. Among these approaches, the most promising dopant for p-type ZnO is group V elements. Ryu *et al.*[5] reported that ZnO layer grown on GaAs substrate exhibited p-type conductivity after post-growth annealing and ascribed the conductivity conversion to the diffusion of As atoms from the substrate into ZnO films. ZnO homojunction light emitting diode with As-doped ZnO as the p-type material has also been demonstrated.[5,11] Kang *et al.*[12] ascribed the p-type conductivity of As-doped ZnO films to the existence of As_{Zn}–$2V_{Zn}$ complex, whose acceptor binding energy is 0.1455 eV determined by using photoluminescence. This value is in good agreement with what reported by Limpijumnong *et al.*[13] based on first-principles calculations.

It is known that surface electrical properties of ZnO could play a crucial role in its overall electrical characteristics. Surface states formed at ZnO surface due to surface atomic reconstruction, structural defects, adsorbates, *etc.;* all may contribute to its electrical properties. For example, Allen *et al.*[14] reported that the existence of oxygen vacancies (V_O) tended to pin Fermi-level close to V_O(+2,0) defect level, which is approximately 0.7 eV below the conduction band minimum, in their studies of Zn-polar face of ZnO wafers. Knowledge about surface electrical properties is thus important for the interpretation of the electrical behavior of ZnO. Nevertheless, only a few studies about the surface electrical properties of p-type ZnO layers have been reported.

In this work, we studied the conductivity conversion of ZnO epitaxial layers grown by pulsed laser deposition on n-type GaAs (001) substrates upon thermal annealing. Structural

[a]*Division of Scientific Research, National Synchrotron Radiation Research Center, Hsinchu 30076, Taiwan. E-mail: liu.weirein@nsrrc.org.tw; chsu@nsrrc.org.tw; Fax: +886 3 578 3813; Tel: +886 3 578 0281 ext. 7130/7118*

[b]*Department of Photonics and Institute of Electro-Optical Engineering, National Chiao Tung University, Hsinchu 30010, Taiwan*

[c]*Department of Physics, Tunghai University, Taichung 40704, Taiwan*

investigation of the as-grown and thermally annealed ZnO films were performed by using X-ray diffraction (XRD); carrier conductivity were conducted by Hall measurement. Secondary ion mass spectrometry (SIMS), and photoluminescence (PL) were employed to characterize the doping species. The spatially resolved surface electrical properties of n- and p-type ZnO epitaxial layers were explored by Kelvin force microscopy (KFM) and electrostatic force microscopy (EFM). The results elucidated the existence of a considerable amount of surface states which played an important role in the electrical properties of the ZnO layers.

Experimental section

ZnO epitaxial films were deposited on Si doped n-type GaAs (001) substrate by pulsed laser deposition (PLD). A beam out of a KrF excimer laser ($\lambda = 248$ nm) at a repetition rate of 10 Hz was focused to produce an energy density ~5–7 J cm^{-2} on a commercial hot-pressed stoichiometric ZnO (5 N) target.[15] The films were deposited at substrate temperature held between 300 and 600 °C without introducing oxygen gas flow; the growth rate is ~0.56 Å s^{-1} and the ZnO layer thickness is ~400 nm. Learning from our previous studies on ZnO films grown on GaAs (111), annealing temperature above 500 °C was necessary to trigger the conversion of carrier type. Similar results have also been reported by other groups.[5,16] On the other hand, annealing at 700 °C or higher leads to serious degradation of surface morphology. This phenomenon is attributed to the serious liberation of As from GaAs substrate, which is confirmed by composition analysis using scanning electron microscopy equipped with energy dispersive spectrometer. Therefore, the annealing temperature of all the samples presented in this work was fixed at 600 °C.

XRD measurements were performed using a four-circle diffractometer at beamline BL13A of the National Synchrotron Radiation Research Center, Taiwan with a wavelength of 1.024 Å. Two pairs of slits located between the sample and the detector yielded a resolution of better than 4×10^{-3} Å^{-1}. Chemical depth profile of the samples was examined by an Atomika SIMS 4500 using Cs^+ as the primary ions and an impact energy of 15 keV. The carrier characteristics of the samples were measured by Hall effect measurements using the four-probe van der Pauw configuration at room temperature (RT). PL measurements were carried out using a He–Cd laser with a wavelength of 325 nm as the pumping source; the emitted light was dispersed by a Triax-320 spectrometer and detected by an UV-sensitive photomultiplier tube. The spatially resolved electrical properties of the ZnO epitaxial layers were characterized by KFM and EFM. A commercial closed-loop-scanner Scanning Probe Microscopy (SPM, Vecco Innova) with a Cr/Pt-coated cantilever, operating in lift-mode with a two-pass technique and dual-frequency mode was employed. An oscillating signal $V_{applied} = V_{ac}\cos(\omega t)$ with an amplitude V_{ac} of 3.5 V and a frequency of 18.72 kHz was applied to the tip; a lift height of 50 nm was used to reduce mechanical-force effect on tip and to remove artificial signals in electric measurements.

In both KFM and EFM measurements, an oscillating voltage $V_{applied}$ is applied directly to the AFM tip and a bias V_{sample} is applied to sample. The tip feels an electrostatic force $F_\omega = \frac{\partial C}{\partial z}(V_{sample} - V_S)V_{applied}$, where $\frac{\partial C}{\partial z}$ and V_S are the vertical derivative of the capacitance and surface potential difference between sample and tip, respectively. KFM measures V_S by adjusting V_{sample} on the tip to minimize F_ω.[17] Quantitative voltage measurements are made by recording the effective V_S as a function of tip position. On the other hand, an EFM image is made of F_ω amplitude recorded as a function of tip position with a fixed V_{sample}. V_S at any location is given by the V_{sample} corresponding to the minimum in the local F_ω *vs.* V_{sample} curve.[17,18] For convenient discussion and the consistence of V_S determined from EFM and KFM results in following sections, KFM images are inversed because of the opposite polarity of applied bias in KFM and EFM measurements.

Results and discussion

Fig. 1(a) illustrates an XRD θ–2θ radial scan along the surface normal of the ZnO layer grown on n-GaAs (001) at 500 °C

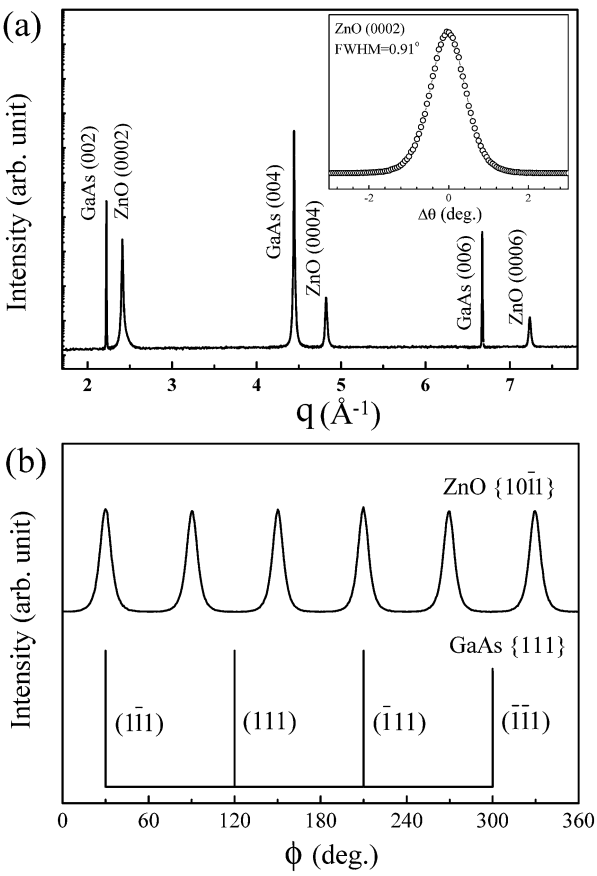

Fig. 1 (a) An XRD radial scan along the surface normal of the ZnO layer grown on n-GaAs (001) at 500 °C followed by post-growth annealing at 600 °C. The inset shows a θ-rocking curve across ZnO (0002) reflection, (b) XRD scans across ZnO (10$\bar{1}$1) and GaAs (111) off-normal reflections of the ZnO layer.

followed by post-growth annealing at 600 °C. Only ZnO (0002), (0004), and (0006) reflections together with the GaAs (002), (004), and (006) reflections were observed, elucidating the ZnO layer is *c*-plane oriented with its [0001] axis parallel to GaAs [001] direction. The mosaicity with a full-width at half-maximum (FWHM) of 1.04°, derived from the ZnO (0002) θ-rocking curve shown in the inset of Fig. 1(a), reveals good crystalline quality of the ZnO layer along the growth direction. The intensity profile of the azimuthal ϕ-scans across ZnO $(10\bar{1}1)$ and GaAs (111) off-normal reflections of the same sample are depicted in Fig. 1(b). Six evenly spaced ZnO $\{10\bar{1}1\}$ diffraction peaks confirm that the ZnO film has 6-fold rotational symmetry against surface normal and is epitaxially grown on GaAs (001). The twist angle (12.7°), derived from the FWHM of the azimuthal ϕ-scan across the ZnO $\{10\bar{1}1\}$ reflection, is much worse than that of *c*-ZnO grown on (111) oriented GaAs, reflecting the unfavorable influence of symmetry mismatch on epitaxial growth. From the angular coincidence of the ZnO $(10\bar{1}1)$ reflection with that of the GaAs $(1\bar{1}0)$ reflection, we determined the relative orientation between ZnO and GaAs as $(0001)[10\bar{1}0]_{ZnO}\|(001)[1\bar{1}0]_{GaAs}$. Because the surface projection of Ga and As dangling bonds are perpendicular to each other on the GaAs (001) surface, the surface anisotropy eliminates the formation of the second rotational variant with 90° in-plane rotation.[19] As to the atomic arrangement on the ZnO/GaAs interface, it requires further investigation and is beyond the scope of this work. Samples grown at different temperatures all showed the same epitaxial orientation. The twist angle decreased monotonically with increasing growth temperature from 300 to 600 °C. The tilt angle, represented by the FWHM of the θ-rocking curve across the ZnO (0002) reflection, also decreased with elevated temperature initially, reached a minimum at ~500 °C, and then increased as grown at 600 °C. In terms of the quality of crystalline structure, the sample grown at 500 °C had the smallest tilt angle and the second smallest twist angle; the one grown at 600 °C had the smallest twist angle and the second smallest tilt angle among all the samples measured. In addition, the one grown at 500 °C had the better electrical properties, larger carrier density, higher mobility, and low resistivity, than the 600 °C one. We thus selected 500 °C grown sample for further optical and electrical studies.

By fitting the angular positions of many Bragg reflections, the lattice parameters of the ZnO layer grown at 500 °C was determined to be $a = 3.252$ Å and $c = 5.203$ Å. As compared with the bulk values, $a = 3.249$ Å and $c = 5.206$ Å determined from a ZnO wafer, the ZnO epitaxial film was almost strain free. The strain of *c*-plane ZnO grown on GaAs is significantly smaller than those grown on *c*-plane sapphire and Si (111) by the same method, which may be attributed to the smaller mismatch in thermal expansion coefficients between ZnO (6.5×10^{-6} K^{-1}) and GaAs (5.39×10^{-6} K^{-1}). Hall effect measurements of the as-deposited samples revealed that electrons were the dominant carriers in all these samples. For the 500 °C grown sample, its carrier density, mobility and resistivity are 5.78×10^{18} cm^{-3}, 24.2 cm^2 V^{-1} s^{-1}, and 4.4×10^{-2} Ω cm, respectively.

After thermal annealing at 600 °C for one hour, the crystalline quality of the ZnO layers exhibited minor improvement, tilt angle = 0.91° and twist angle = 11.8°, as revealed by XRD measurements but the Hall effect results showed drastic changes. The dominant carriers switched to holes for all the annealed samples. The hole concentration, hole mobility, and resistivity of the ZnO layer annealed at 600 °C are 7.6×10^{18} cm^{-3}, 24.6 cm^2 V^{-1} s^{-1} and 3.3×10^{-2} Ω cm, respectively. It is obvious that thermal annealing leads to the conductivity conversion from n- to p-type for the ZnO layers grown on GaAs.

To investigate the cause of conductivity switching and the possible element responsible for such a conversion, we conducted dynamic SIMS measurement on the 600 °C annealed ZnO layer. The secondary ion intensity as a function of depth from the ZnO surface is depicted in Fig. 2. Because the relative sensitive factors of Ga and As in ZnO matrix as well as Zn and O in GaAs matrix are not available in database, we could not quantitatively deduce the concentration of these elements but only probed the trend of concentration variation of individual element. From the steep decrease of the SIMS intensities of various elements, we derived the ZnO layer thickness ~410 nm, which agreed well with the thickness estimated from the growth rate and deposition time. The flat concentration profiles of As and Ga throughout the film manifested their uniform distribution in the ZnO layer. Biswas *et al.* conducted a thorough study on the diffusion behavior of As and Ga from GaAs substrate into MOCVD-grown ZnO films upon post-growth annealing.[20] They found As diffusion prevailed over Ga in the samples annealed at 600 and 700 °C and the observed p-type conductivity was attributed to the As-related acceptors (As_{Zn}–$2V_{Zn}$ complex). For the sample annealed at 800 °C, Ga atoms diffused more than As atoms and they formed shallow donor complex, Ga_{Zn}, compensating the p-type carriers and leading to the reversion of conductivity to n-type. The SIMS results and electrical characteristics of our 600 °C annealed sample resemble that of the 600–700 °C annealed samples reported by Biswas, implying that the change of the electrical properties in our case is mainly ascribed to the diffusion of As atoms. To verify this speculation, we conducted optical and SPM measurements.

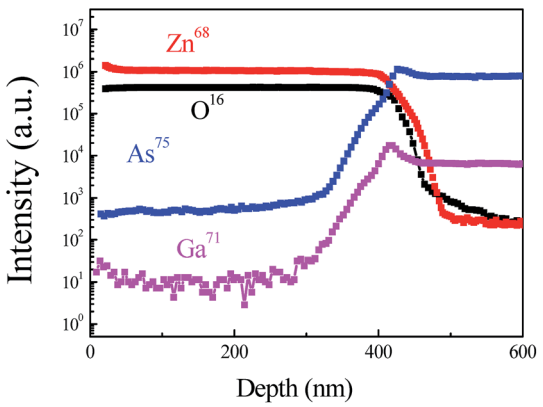

Fig. 2 SIMS depth profile of the ZnO layer grown on n-GaAs (001) at 500 °C followed by post-growth annealing at 600 °C.

The optical properties of the as-deposited and annealed ZnO films were characterized by PL measurements conducted at 13 K, as shown in Fig. 3(a). The spectrum of the as-deposited ZnO has a dominant center peak at 3.362 eV, ascribed to the emission of donor-bound exciton (D^0X). After annealing, the dominant emission was red shifted by ~9 meV to 3.353 eV, which was attributed to the acceptor-bound exciton (A^0X).[21] The red shifting of the near-band edge emission was also reported by other groups and can be regarded as a signature of carrier type conversion.[5,11] The small emission peak at 3.309 eV in the annealed sample was identified as the transition from free electrons to the acceptor state (FA). Acceptor binding energy (ionization energy) can be derived according to $E_A = E_g - E_{FA} + kT/2$, where $E_g = 3.437$ eV is the intrinsic band gap of ZnO,[22] and $E_{FA} = 3.309$ eV is the free electron-acceptor level transition at 13 K. The acceptor binding energy so obtained, 127 meV, agrees well with that of As_{Zn}–$2V_{Zn}$ complex determined by both experimental measurements[8] and first principles calculations (~150 meV) based on density functional theory with local density approximation and ultrasoft pseudopotentials.[12] This result indicates that As_{Zn}–$2V_{Zn}$ complex formed by means of thermal annealing plays an important role in the conversion of carrier type and the change of emission mechanism. The peaks at 3.23 and 3.158 eV are originated from the donor–acceptor pair (DAP) transition and the associated single phonon replica (DAP-1LO).[5,8,23]

To identify the nature of the transition at 3.353 eV, temperature-dependent PL measurements of the annealed ZnO layer was performed and the spectra of near-band edge region are depicted in Fig. 2(c). By fitting the peak positions of the A^0X emission with the Varshni's formula,[24] we determined the binding energy of the A^0X transition to be ~14 meV. This value is larger than the binding energy of D^0X (~10 meV) emission, determined from the as-deposited n-type ZnO layer, implying the faster attenuation of D^0X intensity than A^0X intensity with rising temperature due to thermally activated dissociation.

To understand the influence of dopants on the surface potential of ZnO epi-layers, we performed both KFM and EFM measurements. Prior KFM measurements, the work function of SPM tip, Φ_{Pt}, was calibrated to be 5.650 eV by using a ~0.48 μm thick Pt film grown on glass as a reference. The conventional topographic images of the as-deposited n-type and annealed p-type ZnO layers, shown in Fig. 4(a) and (c), yielded root mean square roughnesses 18.7 nm and 11.9 nm, respectively. The smaller surface roughness of the p-type ZnO layer manifests the improvement of surface planarization by post-growth annealing, in addition to the crystalline improvement revealed by XRD results. Fig. 4(b) and (d) are the KFM images of the n- and p-type ZnO epi-layers, respectively. No apparent correlation between the topography and KFM images was observed in both cases. This ruled out the possibility that KFM contrast was originated from the topographic features. It is noteworthy that the signs of

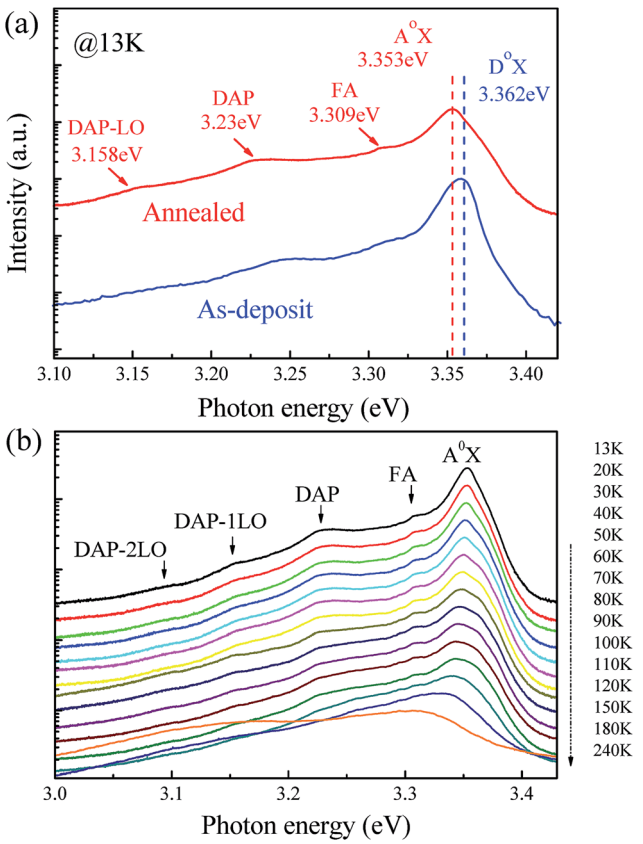

Fig. 3 (a) LT PL spectra of the as-deposited and annealed samples. (b) Temperature-dependent PL spectra of the annealed ZnO layer in NBE region.

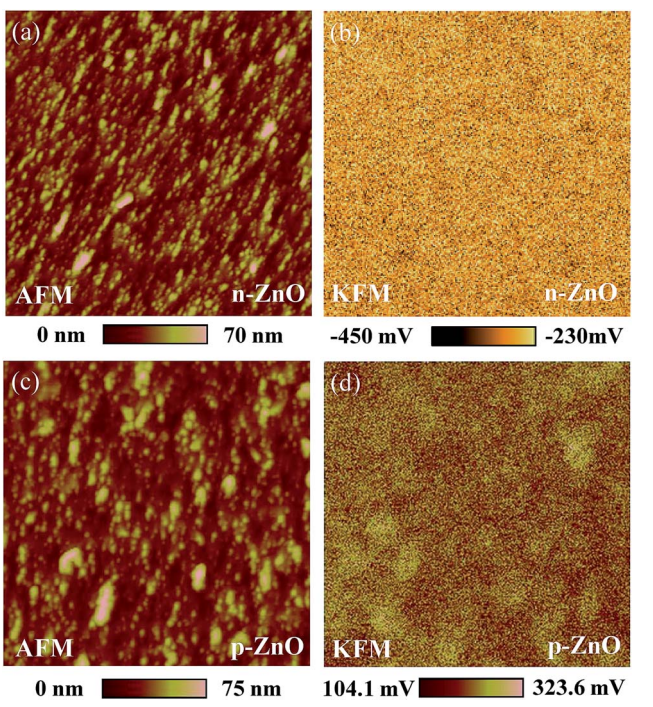

Fig. 4 AFM topography (5 × 5 μm) of (a) the n-type as-deposited ZnO layer, and (c) p-type ZnO layer after annealing at 600 °C. The corresponding KFM images simultaneously recorded with (a) and (c) are shown on (b) and (d), respectively.

V_S are different in the two samples. V_S of the p-type ZnO layer was positive, within the range of 0.214 ± 0.110 V, depending on the probed location. However, for the n-type ZnO layer, its V_S is negative, with a value within −0.340 ± 0.110 V. This result signifies the as-deposited n-type ZnO layer has a work function smaller than that of Pt but the work function of the annealed p-type ZnO layer is larger than that of Pt. This indicates that the observed change of the work function upon annealing reflected the conversion of carrier type induced by dopant ionization.

To further examine the change of V_S with sample conductivity type, we also preformed EFM measurements. EFM probes the amplitude of the electrostatic force on the tip, F_ω, with the sample bias voltage V_{sample} as a parameter. Typically, the spectrum of F_ω as a function of V_{sample} at any given position on the sample exhibits a V-shape profile, as shown in Fig. 5, and the value of V_{sample} associated with the minimum in F_ω equals to the V_S at that position.[17,18] Fig. 5(a) and (b) illustrate the local spectra of F_ω recorded at two specific locations, which show distinct contrast in the corresponding KFM images shown in the up-right corners, on the as-deposited and annealed samples, respectively. In the spectra taken at points A and B on the n-ZnO layer, F_ω reached the minimum at the same value $V_{sample} \sim -0.394$ V, implying that both points had the same V_S value and the work function of the n-type ZnO is lower than that of Pt. In contrast, the values of V_{sample} with minimal F_ω at points C and D in p-type ZnO layer are significantly different, 0.151 and 0.308 V, respectively, revealing the nonuniformity in V_S distribution, which may be attributed to the inhomogeneous diffusion of As caused by structural defects, *e.g.* vacancies, dislocations, grain boundaries, *etc.* Furthermore, the positive V_{sample} to nullify F_ω of the annealed sample manifests that the p-type ZnO layer has a larger work function than that of Pt.

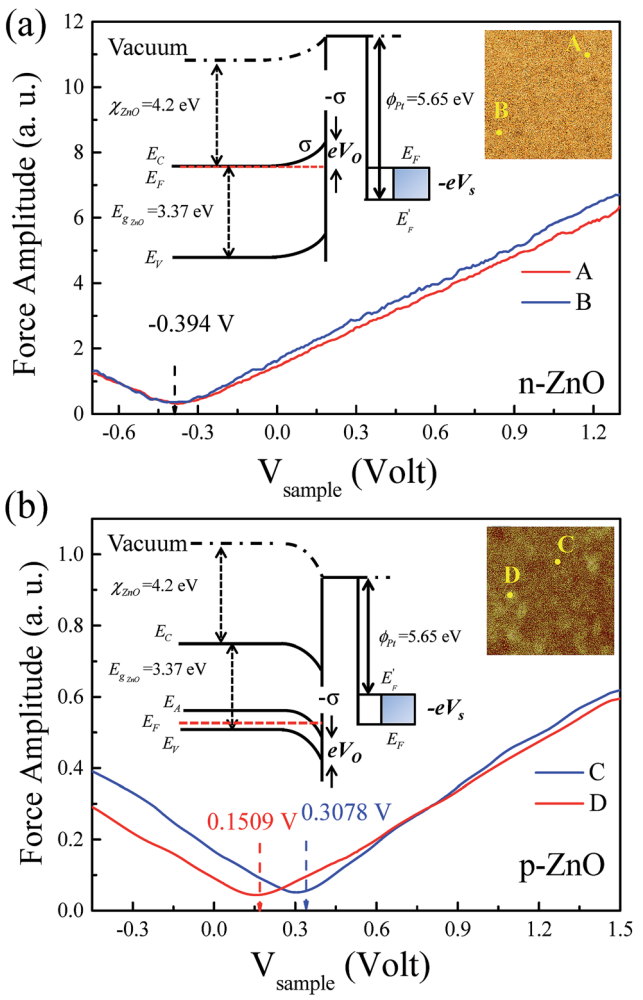

Fig. 5 (a) The local electrostatic force F_ω *vs.* V_{sample} curves of the n-type ZnO layer recorded at points A and B, marked on the KFM image depicted in the inset shown in the upper right corner. Similar spectra of the annealed p-type ZnO layer taken at points C and D are shown in (b). The schematic band diagrams of the n- and p-type ZnO layers are shown as the insets in the respective figures.

According to the V_S deduced from KFM and EFM results and given electrical affinity of ZnO, χ_{ZnO} = 4.2 eV,[25] the band diagrams of both n- and p-type ZnO layers were constructed, as depicted in the insets of Fig. 5. At the surface of the n-type ZnO layer where V_S is −0.394 V, its Fermi level (E_F) is located at 1.06 eV below conduction-band minimum (CBM) at the surface; for the p-type ZnO, taking V_S = 0.23 ± 0.078 V from the EFM results, E_F at the surface is located at 1.68 ± 0.079 eV below CBM, or equivalently 1.69 ± 0.079 eV above valence-band maximum (VBM) with E_g = 3.37 eV adopted as the ZnO band gap at RT.

It is noted that the E_F difference between n- and p-type ZnO epi-layers, 0.589–0.75 eV, is much smaller than ZnO band gap 3.37 eV, implying the existence of surface states near the mid gap. These surface states would induce band bending at the band edges and consequently Fermi-level pinning. Similar results have been reported by Allen *et al.*[14] who found that E_F of n-type ZnO was pinned in the band gap due to interface states caused by structural defects.

To estimate the density of surface states of the n- and p-type ZnO epi-layers, a uniform charge model in the depletion region was applied.[26] According to the model, surface charge density is expressed as $\sigma = \pm\sqrt{|2eN_D\varepsilon_0\varepsilon_r V_0|}$, where N_D (N_A for p-type ZnO) denotes the doping density coming from the ionized donors in the depletion region, ε_r = 7.77 is the relative dielectric constant of ZnO,[27] and the band-bending voltage V_0 can be written by $eV_0 = \Phi_{Pt} - \chi_{ZnO} - eV_S - (E_C - E_F)$. For the n-type ZnO layer, its E_F is suggested to lie in the conduction band, *i.e.* $E_F \sim E_C$, because the electron concentration $n = 5.78 \times 10^{18}$ cm^{-3} determined from the Hall effect measurements is larger than the ZnO effective conduction band density of states calculated from $N_C = 2\left(\frac{2\pi m_e^* kT}{h^2}\right)^{3/2} \approx 2.72 \times 10^{18}$ cm^{-3}, where k is the Boltzmann constant, T is temperature, h is the Planck constant, and $m_e^* = 0.24m_0$ denotes electron effective mass.[28] V_0 is thus determined to be 1.06 V. Furthermore, N_D is approximated by the electron density determined from the Hall measurements 5.78×10^{18} cm^{-3}, as $N_D \gg N_A$. The surface charge density of n-type ZnO layer is then calculated to be $\sigma \sim -7 \times 10^{12}$ e cm^{-2}.

Similar calculation was also carried out for the p-type ZnO layer. In order to calculate surface state density, we need to

determinate the concentration of acceptors, N_A, which can be expressed as[29]

$$\frac{p(p+N_D)}{N_A-N_D-p}=\frac{N_V}{g}\exp\left(-\frac{E_A}{kT}\right)\approx\frac{\frac{p^2}{N_A}}{1-\frac{p}{N_A}},\ \text{as } N_A\gg N_D$$

where the acceptor activation energy E_A, 127 meV and hole concentration p, 7.6×10^{18} cm^{-3} were obtained from our PL and Hall results, respectively, N_D is the concentration of compensating donors, g denotes acceptor degeneracy and is assumed to be 4, $N_V=2\left(\frac{2\pi m_h^* kT}{h^2}\right)^{3/2}\approx1.134\times10^{19}$ cm^{-3} is the effective valence band density of states, where $m_h^*\approx m_0$ is hole effective mass.[3] With the numbers given above, we obtained $N_A\approx1.24\times10^{21}$ cm^{-3}. Following $E_F-E_V=kT\ln\left(\frac{N_V}{N_A}\right)$, we obtained $E_F\sim E_V$ due to the negative $kT\ln\left(\frac{N_V}{N_A}\right)$ value. With the average value of V_S, 0.23 V, the average V_0 of the p-type ZnO layer obtained from EFM is about −1.69 V; the surface charge density of the p-type ZnO layer is thus $\sim1.3\times10^{14}$ e cm^{-2}.

These results revealed the shift of E_F between the n- and p-type ZnO layers was caused by the development of the depletion charge varying from $\sim-7\times10^{12}$ to 1.3×10^{14} e cm^{-2}; the corresponding state density was $\sim2.2\times10^{14}$ cm^{-2} eV^{-1}.[30] Bard *et al.*[31] reported that a surface state density as low as $\sim1\times10^{12}$ cm^{-2} was sufficient to result in band bending and Fermi level pinning. In n- and p-type GaN epi-layers, Barbet *et al.*[26] showed that the existence of a surface state density of a few 10^{13} states cm^{-2} eV^{-1} near the mid gap caused E_F pinning and band bending. In that case, E_F of n-type GaN was found 1.34 eV below CBM and p-type GaN's was 1.59 eV above VBM. Therefore, the observed small E_F difference between the n- and p-type ZnO epitaxial layers implies Fermi level pinning at the surface of the n- and p-type ZnO epitaxial layers caused by the existence of high density of surface states close to the ZnO mid-gap. Because the work function of chosen standard Pt 5.65 eV is close to the ZnO mid gap 5.89 eV, which is calculated by $\chi_{ZnO}+0.5\,E_g$, even though the Fermi levels of both n- and p-type ZnO are pinned near the mid gap and their difference is small, the work function of the ZnO layer changed across that of Pt upon annealing.

Conclusions

Wurtzite ZnO epitaxial layers were grown on n-type cubic GaAs (001) substrates by pulsed laser deposition (PLD). The epitaxial relationship between the ZnO layers and GaAs follows $(0001)\langle10\bar{1}0\rangle_{ZnO}\|(001)\langle1\bar{1}0\rangle_{GaAs}$ as determined by X-ray diffraction (XRD). Post-growth annealing of the as-deposited n-type ZnO epitaxial layer lead to carrier type switching from electron to hole, which was attributed to the arsenic diffusion from the substrate. The surface electrical properties of the ZnO layers characterized by KFM and EFM revealed the existence of high surface state density of a few 10^{14} cm^{-2} eV^{-1} close to the ZnO mid-gap. Fermi level are found at 1.014 eV below CBM and 1.612–1.769 eV above VBM for n- and p-type ZnO layers, respectively. As compared with the hole concentration of ZnO doped with other group-V elements, *e.g.* N,[3] our result seems to be high. However, surface effects are known to particularly important in affecting the electrical properties of p-type ZnO, *e.g.* surface conductivity or the development of depletion layer caused by chemical adsorption.[32,33] Surface conduction effect, mixed conduction, or photoconduction are possible causes of the obtained low Hall voltage and consequently the high hole concentration. In this study, it is demonstrated that the existence of surface states indeed has a great influence on the electrical properties of ZnO films.

Acknowledgements

The National Science Council (NSC) of Taiwan supported this work under Contracts NSC 102-2112-M-213-004-MY3, NSC 100-2112-M-213-002-MY3, and NSC 102-2112-M-009-016-MY3.

References

1 S. B. Zhang, S. H. Wei and A. Zunger, *Phys. Rev. B: Condens. Matter Mater. Phys.*, 2001, **63**, 075205.
2 D. C. Look, J. W. Hemsky and J. R. Rizelove, *Phys. Rev. Lett.*, 1999, **82**, 2552.
3 D. C. Look, D. C. Reynolds, C. W. Litton, R. L. Jones, D. B. Eason and G. Cantwell, *Appl. Phys. Lett.*, 2002, **81**, 1830.
4 K. K. Kim, H. S. Kim, D. K. Hwang, J. H. Lim and S. J. Park, *Appl. Phys. Lett.*, 2003, **83**, 63.
5 (*a*) Y. R. Ryu, S. Zhu, D. C. Look, J. M. Wrobel, H. M. Jeong and H. W. White, *J. Cryst. Growth*, 2000, **216**, 330; (*b*) Y. R. Ryu, T. S. Lee, J. A. Lubguban, H. W. White, B. J. Kim, Y. S. Park and C. J. Youn, *Appl. Phys. Lett.*, 2006, **88**, 241108; (*c*) Y. R. Ryu, T. S. Lee and H. W. White, *Appl. Phys. Lett.*, 2003, **83**, 87.
6 S. Chu, J. H. Lim, L. J. Mandalapu, Z. Yang, L. Li and J. L. Liu, *Appl. Phys. Lett.*, 2008, **92**, 152103.
7 Y. J. Zeng, Z. Z. Ye, J. G. Lu, W. Z. Xu, L. P. Zhu, B. H. Zhao and S. Limpijumnong, *Appl. Phys. Lett.*, 2006, **89**, 042106.
8 H. S. Kang, B. D. Ahn, J. H. Kim, G. H. Kim, S. H. Lim, H. W. Chang and S. Y. Lee, *Appl. Phys. Lett.*, 2006, **88**, 202108.
9 G. D. Yuan, Z. Z. Ye, L. P. Zhu, Q. Qian, B. H. Zhao and R. X. Fan, *Appl. Phys. Lett.*, 2005, **86**, 202106.
10 J. G. Lu, Y. Z. Zhang, Z. Z. Ye, L. P. Zhu, L. Wang, B. H. Zhao and Q. L. Liang, *Appl. Phys. Lett.*, 2006, **88**, 222114.
11 J. C. Sun, J. Z. Zhao, H. W. Liang, J. M. Bian, L. Z. Hu, H. Q. Zhang, X. P. Liang, W. F. Liu and G. T. Du, *Appl. Phys. Lett.*, 2007, **90**, 121128.
12 H. S. Kang, G. H. Kim, D. L. Kim, H. W. Chang, B. D. Ahn and S. Y. Lee, *Appl. Phys. Lett.*, 2006, **89**, 181103.
13 S. Limpijumnong, S. B. Zhang, S. H. Wei and C. H. Park, *Phys. Rev. Lett.*, 2004, **92**, 155504.
14 M. W. Allen and S. M. Durbin, *Appl. Phys. Lett.*, 2008, **92**, 122110.
15 (*a*) W. R. Liu, W. F. Hsieh, C. H. Hsu, K. S. Liang and F. S. S. Chien, *J. Appl. Crystallogr.*, 2007, **40**, 924; (*b*) W. R. Liu, B. H. Lin, C. C. Kuo, Y. H. Li, W. F. Hsieh, C. H. Hsu, W. C. Lee, M. Hong and J. Kwo, *CrystEngComm*,

2012, **14**, 1665; (*c*) W. R. Liu, B. H. Lin, C. C. Kuo, W. C. Lee, M. Hong, J. Kwo, C. H. Hsu and W. F. Hsieh, *CrystEngComm*, 2012, **14**, 8103.

16 (*a*) J. Sun, H. Liang, J. Zhao, Q. Feng, J. Bian, Z. Zhao, H. Zhang, Y. Luo, L. Hu and G. Du, *Appl. Surf. Sci.*, 2008, **254**, 7482; (*b*) Y.-C. Huang, L.-W. Weng, W.-Y. Uena, S.-M. Lan, Z.-Y. Li, S.-M. Lia, T.-Y. Lin and T.-N. Yang, *J. Alloys Compd.*, 2011, **509**, 1980; (*c*) Y.-C. Cheng, Y.-S. Kuo, Y.-H. Li, J.-J. Shyue and M.-J. Chen, *Thin Solid Films*, 2011, **519**, 5558.

17 G. Koley and M. G. Spencer, *J. Appl. Phys.*, 2001, **90**, 337.

18 J. Moser, A. Verdaguer, D. Jiménez, A. Barreiro and A. Bachtold, *Appl. Phys. Lett.*, 2008, **92**, 123507.

19 W. G. Schmidt, F. Bechstedt and J. Bernholc, *Appl. Surf. Sci.*, 2002, **190**, 264.

20 P. Biswas, N. N. Halder, S. Kundu, P. Banerji, T. Shripathi and M. Gupta, *AIP Adv.*, 2014, **4**, 057108.

21 A. Teke, Ü. Özgür, S. Dogan, X. Gu, H. Morkoç, B. Nemeth, J. Nause and H. O. Everitt, *Phys. Rev. B: Condens. Matter Mater. Phys.*, 2004, **70**, 195207.

22 B. K. Meyer, H. Alves, D. M. Hofmann, W. Kriegseis, D. Forster, F. Bertram, J. Christen, A. Hoffmann, M. Straßburg, M. Dworzak, U. Haboeck and A. V. Rodina, *Phys. Status Solidi B*, 2004, **241**, 231.

23 F. X. Xiu, Z. Yang, L. J. Mandalapu and J. L. Liu, *Appl. Phys. Lett.*, 2006, **88**, 152116.

24 D. S. Jiang, H. Jung and K. Ploog, *J. Appl. Phys.*, 1988, **64**, 1371.

25 L. J. Brillson, *Zinc Oxide Materials for Electronic and Optoelectronic Device Applications*, ed. C. W. Litton, D. C. Reynolds and T. C. Collins, Wiley, Chichester, 2011, ch. 4, p. 87.

26 S. Barbet, R. Aubry, M.-A. Di Forte-Poisson, J.-C. Jacquet, D. Deresmes, T. Mélin and D. Théron, *Appl. Phys. Lett.*, 2008, **93**, 212107.

27 Ü. Özgür, Y. I. Alivov, C. Liu, A. Teke, M. A. Reshchikov, S. Doğan, V. Avrutin, S.-J. Cho and H. Morkoç, *J. Appl. Phys.*, 2005, **98**, 041301.

28 S. Adachi, *Handbook on Physical Properties of Semiconductors: II–VI Compound Semiconductors*, Kluwer Academic Publishers, Boston, 2004, ch. 5, p. 82.

29 P. Kozodoy, H. Xing, S. P. DenBaars, U. K. Mishra, A. Saxler, R. Perrin, S. Elhamri and W. C. Mitchel, *J. Appl. Phys.*, 2000, **87**, 1832.

30 S. M. Sze, *Physics of Semiconductor Devices*, Wiley, New York, 2nd edn, 1981, p. 275.

31 A. J. Bard, A. B. Bocarsly, F.-R. F. Fan, E. G. Walton and M. S. Wrighton, *J. Am. Chem. Soc.*, 1980, **102**, 3671.

32 C. H. Swartz, *J. Mater. Res.*, 2012, **27**, 2205.

33 O. Schmidt, A. Geis, P. Kiesel, C. G. V. De Walle, N. M. Johnson, A. Bakin, A. Waag and G. H. Döhler, *Superlattices Microstruct.*, 2006, **39**, 8.